

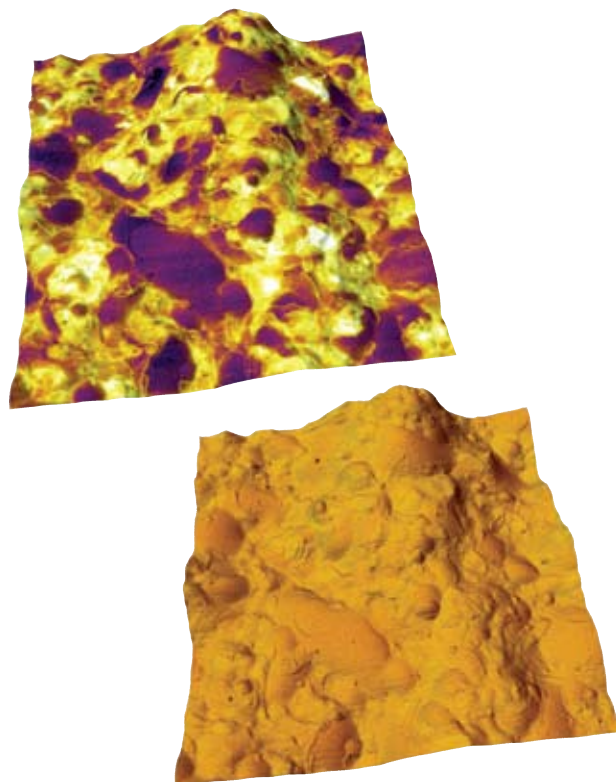
# Bimodal Dual AC™ Imaging

An exclusive new measurement ability, Dual AC, has been developed by Asylum Research for use on the MFP-3D™ and Cypher™ AFMs. Since its introduction, the number of applications for Dual AC has increased dramatically. This note will give you an introduction to bimodal imaging, just one of many Dual AC techniques that can be performed on Asylum's AFMs.

## Background

Dual AC imaging encompasses a wide variety of techniques. We have broken down these various imaging techniques to specifically describe the mode for different applications. The table below explains the various Dual AC techniques along with the software settings needed for imaging. For this application note, only bimodal Dual AC imaging will be discussed.

Figure 1: Bimodal Dual AC 2nd mode amplitude overlaid on rendered AFM topography (top) and fundamental phase image overlaid on topography (bottom) of multi-component surf wax. Notice the high contrast visible in the bimodal Dual AC image and the relative lack of contrast in the fundamental phase, 4µm scan.



Technique	Description	MFP-3D Software Settings			
		Frequency 1- $f_1$	Frequency 2- $f_2$	Drive 1-2	Mode: Drive
Bimodal <sup>1</sup>	Drive the 1st and 2nd resonance.	At or near fundamental resonance	At or near 2nd resonance	On-On	Dual AC: Shake
MFM <sup>2</sup>	Bimodal with special operating parameters and a magnetic cantilever.	At or near fundamental resonance	At or near 2nd resonance	On-On	Dual AC: Shake
Passive bimodal	Similar to bimodal, but the 2nd resonance is only monitored, not driven.	At or near fundamental resonance	At or near 2nd resonance	On-Off	Dual AC: Shake
Active harmonic	Similar to bimodal, but a higher harmonic driven.	At or near fundamental resonance	$f_2 = N \times f_1$ , where N is an integer	On-On	Dual AC: Shake
Passive harmonic	Higher harmonic is simply monitored, not driven.	At or near fundamental resonance	$f_2 = N \times f_1$ , where N is an integer	On-Off	Dual AC: Shake
DART	By driving at one frequency below resonance ( $A_1$ ) and another above ( $A_2$ ), the $A_2 - A_1$ gives an error signal we can use to track the resonance frequency changes.	Slightly below fundamental resonance ( $A \sim A_{max}/2$ )	Slightly above fundamental resonance ( $A \sim A_{max}/2$ )	On-On	Dual AC to Shake
DART-PFM <sup>3</sup>	Piezoresponse Force Microscopy technique using the above.	Slightly below fundamental resonance ( $A \sim A_{max}/2$ )	Slightly above fundamental resonance ( $A \sim A_{max}/2$ )	On-On	PFM: Dual AC to Chip

## Bimodal Dual AC Imaging – How it Works

Bimodal Dual AC imaging provides enhanced contrast for materials properties (Figure 1) by taking advantage of the flexibility and power of the digital signal processing within the ARC2™ controller. The idea behind this is simple. Cantilevers are extended mechanical objects and have many different flexural resonant frequencies. In the past, AC atomic force microscopes have typically excited one of those modes, usually the lowest frequency, or “fundamental” mode and then used the amplitude or frequency of that mode as the input for a feedback system that controls the tip-sample separation.<sup>4,5</sup> When the amplitude of the fundamental motion is used, the term “Amplitude Modulated AFM”<sup>6</sup> (AM-AFM) has been employed.

A plucked guitar string has higher flexural resonances that are *harmonic*, meaning that if the fundamental mode is at a frequency  $f_0$ , the next resonance is at  $2f_0$ , the next is at  $3f_0$  and so on. For all but a few very specialized types,<sup>7,8</sup> cantilever resonant frequencies are *non-harmonic*. Butt and Jaschke<sup>9</sup> as well as Sarid<sup>10</sup> give nice reviews of cantilever mechanics. Figure 2 gives the theoretical resonant frequencies for diving board shaped cantilevers for the first few resonant frequencies. The measured resonant frequencies for two representative cantilevers, the Olympus AC-240 (for air imaging) and Olympus Bio-Lever (for fluid imaging) are also listed.

One of the simplest methods for looking at the effect of higher modes is to drive them directly, using the same machinery set-up as that used in AC imaging.<sup>11</sup> As with AC imaging using the first resonant frequency, the amplitude of the cantilever measured at the drive frequency is used as the error signal in a feedback loop. In reference 8, Stark et al. observed enhanced phase contrast on a sample using the third resonant frequency of a triangular cantilever. Crittenden et al. have also explored using higher harmonics for imaging because the response of the higher harmonics is sharper than the response of the fundamental resonance.<sup>12</sup>

If the periodic repulsive interactions between the tip and sample are nonlinear, they will couple motion into higher harmonics.<sup>13,14,15,16</sup> This can provide information about the mechanical properties of the sample. During a single AM-AFM vibrational cycle, the tip typically samples a range of forces, from the long range attractive to the short range repulsive. If the tip interacts with the short ranged repulsive forces, information about the mechanical properties of the sample can be obtained.

For single oscillation mode imaging, if the phase shift is positive, it is customary to refer to the imaging mode as “net attractive” or simply “attractive”. If the phase shift is negative, the mode is referred to as “repulsive”. Recently, Rodriguez and Garcia<sup>17</sup> published a theoretical simulation of a non-contact, attractive

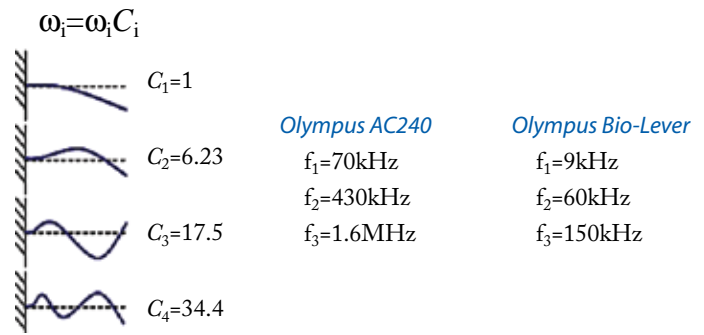


Figure 2: Theoretical resonant frequencies of diving board shaped cantilevers in terms of the fundamental,  $\omega_1$ , as well as resonant frequencies for the Olympus AC240 and Bio-Levers. In these cases, the theoretical predictions typically agree with the measured results to well within 10%.

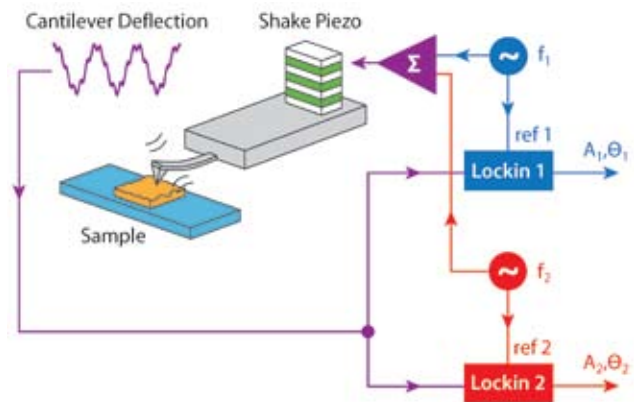


Figure 3: In bimodal Dual AC, the cantilever is both driven and measured at two (or more) frequencies. The sinusoidal “shake” voltage is a sum of voltages at frequencies  $f_1$  and  $f_2$ . The cantilever deflection then contains information at both of those frequencies, as shown in the red curve. The amplitude and phase at the two frequencies are then separated again by the two lockins and passed on to the controller. The controller can use one or both of the resonant frequencies to operate a feedback loop.

mode technique where the cantilever was driven at its two lowest resonant frequencies. In their simulations, they observed that the phase of the second mode had a strong dependence on the Hamaker constant of the material being imaged, implying that this technique could be used to extract chemical information about the surfaces being imaged. Other work by Garcia’s group has also demonstrated that the compositional sensitivity of an AFM is enhanced by the simultaneous excitation of its first two normal resonant frequencies 1–2.<sup>18</sup>

Figure 3 shows the basic idea of bimodal Dual AC imaging mode using two typically non-harmonic resonant frequencies of a cantilever. The cantilever is driven with a linear combination of sinusoidal voltages, at or near their resonant frequencies,  $f_1$  and  $f_2$ . This signal is used to drive the base of a cantilever with a “shake” piezo. The experiments reported here were repeated with a magnetically activated cantilever<sup>19</sup> with similar results. It is expected that other actuation methods where two drive waveforms can be summed

will prove as effective. The resulting motion of the cantilever is measured with a position sensor. This signal in turn is used as the input for two separate lock-in amplifiers, where the function generator  $f_1$  is used as a reference for one lockin and  $f_2$  is used as a reference for the other. The output of the lockin amplifiers, including the Cartesian in-phase and quadrature pairs  $(x_1, y_1, x_2, y_2)$  and polar amplitude and phase  $(A_1, \theta_1, A_2, \theta_2)$  representations of the cantilever motion at the two or more frequencies can then be passed on to the controller where they can be displayed, saved, combined with other signals, and used in feedback loops.

### Feedback

As with conventional AC imaging, the amplitude of the cantilever is used as the feedback error signal. There is a difference here, however, since there are two amplitudes – one at each drive frequency. The initial results we present use the amplitude of the fundamental frequency  $A_1$  as the feedback error signal and fundamental phase  $\theta_1$ , the second resonant frequency amplitude  $A_2$ , and phase  $\theta_2$  as “carry-along” signals. Reversing this and using the higher resonant frequency amplitude as a feedback and carrying the fundamental amplitude and phase along can also yield interesting results. The sum of all of the amplitudes as the error signal also allowed stable imaging.

An interesting feature of this measurement is that the signal processing can be performed on the same cantilever deflection data stream for each flexural mode. With a digital lockin implementation, for example, this implies that the same position sensitive detector and analog to digital converter (as long as it has sufficient bandwidth for the higher mode) can be used to extract information regarding the distinct resonant frequencies.

## Bimodal Image Examples

### Graphite

Figure 4 shows a 30 $\mu$ m image made on a highly oriented pyrolytic graphite (HOPG) surface.<sup>20</sup> The cantilever was a silicon AC-240 cantilever from Olympus. It was driven at the fundamental ( $f_1 \sim 69.5$  kHz,  $A_1 \sim 8$  nm) and second resonant frequency ( $f_2 \sim 405$  kHz,  $A_2 \sim 8$  nm). No significant differences were observed for similar cantilevers imaging the graphite surface. The Z-feedback loop was operated using the fundamental amplitude  $A_1$  as the error signal. The topography (A) shows the expected terraces separated by single or multiple atomic steps. The first mode amplitude (B) channel resembles a high-pass filtered image of the topography. The fundamental phase image (C) shows an average phase lag of  $\sim 34^\circ$  and very little variation ( $\leq 1^\circ$  standard deviation), implying that the cantilever was consistently in repulsive mode. Again, there is very little contrast in the fundamental phase image. The second mode amplitude image (D), however, has significant contrast, with broad patches

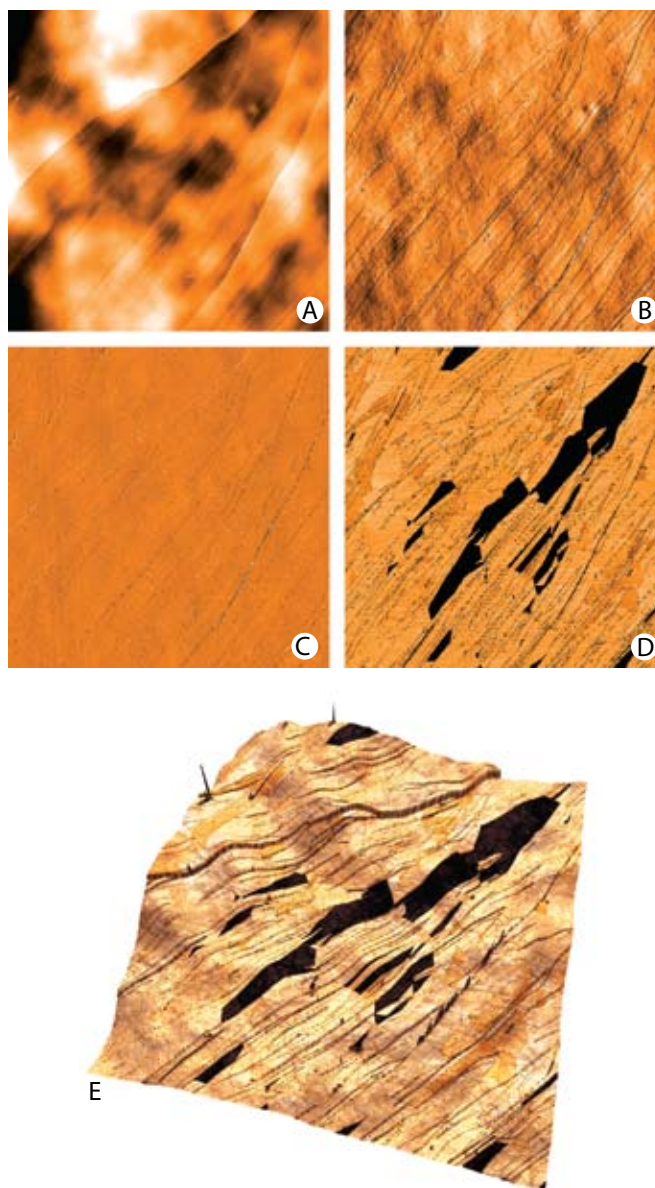


Figure 4: Graphite images A-D showing different imaging modes (see text) and bimodal Dual AC 2nd mode amplitude overlaid on AFM rendered topography (E), 30 $\mu$ m scan.

showing regions where  $A_2$ , the second mode amplitude, was reduced by tip-sample interactions. A three dimensional rendering of the surface topography (A) with the second resonant frequency amplitude (D) “painted” onto the rendered surface (E) allows the high contrast second mode data to be correlated with the topography. Although (E) makes it clear there is a high degree of correlation, there are also boundaries in the second mode amplitude that seem to have no connection to topographical features.

### DNA in Fluid

Bimodal Dual AC imaging also works well for AM-AFM imaging in fluids. A high density  $\lambda$ -digest deoxyribonucleic acid (DNA) sample<sup>21</sup> was prepared in a dense mat on freshly cleaved mica. Figure 5 shows the response of a 60 $\mu$ m long Olympus

Bio-Lever in fluid being driven at its fundamental resonance ( $f_1 \sim 8.5\text{kHz}$ ,  $A_1 \sim 8\text{nm}$ ) and at its second mode ( $f_2 \sim 55\text{kHz}$ ,  $A_2 \sim 5\text{nm}$ ) in the DNA buffer solution. The topography (A) shows a dense mat of material on the surface with no clear strands of DNA visible. Similarly, the fundamental amplitude (B), the channel used for the feedback error signal, shows no particular structure. The fundamental phase channel (C) shows subtle contrast between the background and a structure that shows hints of being strands of DNA molecules. The second mode amplitude (D) shows clear, high contrast images of the same DNA strands. The strands appear dark, corresponding to an increased dissipation. This is consistent with the DNA strands being slightly less bound to the sample and thus able to absorb some of the second resonant frequency energy. Again, rendering the topography in three dimensions and painting the second mode amplitude on top (E) allowed the topography and second mode amplitude to be spatially correlated.

## Conclusion

By measuring the cantilever response at two different frequencies, it is possible to look at the difference in, for example, the phase signals at the fundamental drive frequency and at a higher mode drive frequency. In the future, this may help with extracting frequency-dependent mechanical properties of the sample. Significant contrast differences can be observed by operating a repulsive mode AM-AFM cantilever at more than one of its flexural resonances. As research continues, we're constantly learning more about bimodal Dual AC. Contact Asylum Research to learn about the latest discoveries and applications on this technique.

## References

1. R. Proksch, Applied Physics Letters 89, 113121 (2006).
2. J. Li, J. Cleveland, R. Proksch, Applied Physics Letters 94, 163118 (2009).
3. B.J. Rodriguez, C. Callahan, S.V. Kalinin, and R. Proksch, Nanotechnology 18, 475504 (2007).
4. G. Binnig, C.F. Quate, and C. Gerber, Physical Review Letters 56 (9), 930 (1986).
5. Y. Martin, C. C. Williams, and H. K. Wickramasinghe, Journal of Applied Physics 61 (10), 4723 (1987).
6. R. Garcia and R. Perez, Surface Science Reports 47 (6-8), 197 (2002).
7. O. Sahin, G. Yaralioglu, R. Grow, S. F. Zappe, A. Atalar, C. Quate, and O. Solgaard, Sensors and Actuators A-Physical 114 (2-3), 183 (2004).
8. O. Sahin, C. F. Quate, O. Solgaard, and A. Atalar, Physical Review B 69 (16) (2004).
9. H.J. Butt and M. Jaschke, Nanotechnology 6 (1), 1 (1995).
10. D. Sarid, Scanning Force Microscopy. (Oxford University Press, 1990).
11. R.W. Stark, T. Drobek, and W.M. Heckl, Applied Physics Letters 74 (22), 3296 (1999).
12. S. Crittenden, A. Raman, and R. Reifengerger, Physical Review B 72 (23) (2005).

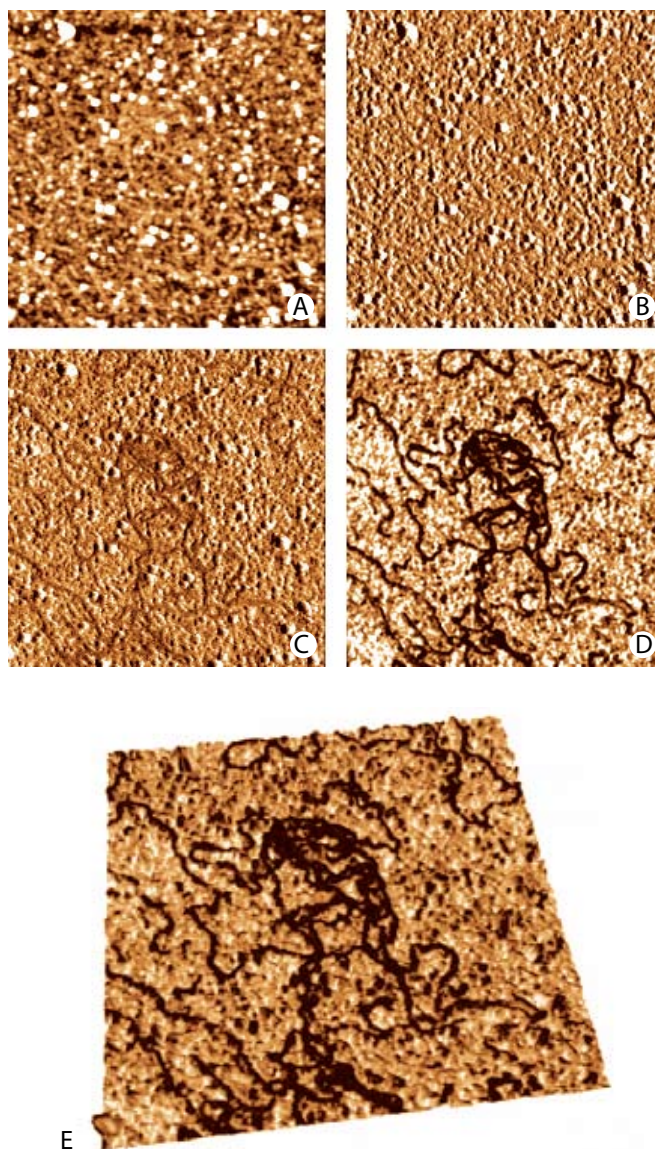


Figure 5: (A) topography, (B) fundamental amplitude, (C) fundamental phase, (D) bimodal Dual AC second mode amplitude of DNA, 750nm scan. (E) Second mode amplitude data overlaid on rendered AFM topography.

13. M. Stark, R. W. Stark, W. M. Heckl, and R. Guckenberger, Proceedings of the National Academy of Sciences of the United States of America 99 (13), 8473 (2002).
14. R. Hillenbrand, M. Stark, and R. Guckenberger, Applied Physics Letters 76 (23), 3478 (2000).
15. R. W. Stark and W. M. Heckl, Review of Scientific Instruments 74 (12), 5111 (2003).
16. R. W. Stark, Nanotechnology 15 (3), 347 (2004).
17. T. R. Rodriguez and R. Garcia, Applied Physics Letters 84 (3), 449 (2004).
18. N.F. Martinez, S. Patil, J.R. Lozano and R. Garcia, APL 89, 153115 (2006).
19. A. Buguin, O. Du Roure, and P. Silberzan, Applied Physics Letters 78 (19), 2982 (2001).
20. HOPG Graphite. SPI Incorporated, West Chester, PA.
21. Sigma 50 ug/ml, imaged in 40mM HEPES, 5mM NiCl<sub>2</sub> with a pH of 6.6-6.8.